Journal of Cell Science 104, 339-352 (1993)
Printed in Great Britain © The Company of Biologists Limited 1993

Composite microtubules of the axon: quantitative analysis of tyrosinated and acetylated tubulin along individual axonal microtubules

Anthony Brown, Yan Li, Theresa Slaughter and Mark M. Black*

Department of Anatomy and Cell Biology, Temple University School of Medicine, 3400 North Broad Street, Philadelphia, PA 19140, USA

*Author for correspondence

SUMMARY

We have shown previously, using immunoelectron microscopy, that axonal microtubules (MTs) are composite, consisting of distinct domains that differ in their content of tyrosinated α-tubulin (tyr-tubulin). Here, we extend these studies using a novel preparation that permits visualization of individual axonal MTs over distances of several tens of micrometres using conventional immunofluorescence procedures. Neurons are cultured on a substratum of poly-lysine and laminin and then extracted with a MT stabilizing solution containing Triton X-100 and NaCl. These extraction conditions cause a loosening of the axonal MT array so that individual MTs separate from each other for variable distances along their length. We call this phenomenon fraying. Within the axon shaft, individual MTs can often be traced for several tens of micrometres, but fraying is most extensive in the distal 100-200 μm of the axon, where individual MTs can frequently be traced for distances of 50 to 100 μm or more to their plus ends. In some cases MTs separate completely from the axon, permitting visualization of both of their ends. Double-staining of frayed preparations with various combinations of antibodies against tyr-tubulin, acetylated α-tubulin (Ac-tubulin) or β-tubulin, clearly revealed the composite nature of axonal MTs. Composite MTs consisted of two distinct domains, one that was relatively rich in tyr-tubulin and poor in Ac-tubulin, and the other that was relatively poor in tyr-tubulin and rich in Ac-tubulin. The transition between these domains was relatively abrupt, with the tyr-tubulin-rich domain extending from the transition to the plus-end of the MT. Quantitative analyses of fluorescence intensity along individual MTs using digital image processing revealed that the relative amount of tyr-tubulin increased by approximately 800% across the transition, whereas the relative amount of Ac-tubulin decreased by approximately 60%. Within the tyr-tubulin-rich domains, the relative amount of tyr-tubulin was generally not constant, but increased from the transition to the plus-end of the MT in a nonlinear manner. We propose that the specific pattern of variation in the extent of post-translational modification along an individual MT represents a snapshot of that polymer's growth history.

Key words: tyrosinated tubulin, acetylated tubulin, microtubules, microtubule dynamics, axon

INTRODUCTION

In a previous study, we demonstrated that individual axonal microtubules (MTs) are composite, consisting of two distinct domains that differ in their content of post-translationally modified tubulin subunits and in their stability properties (Baas and Black, 1990). One domain stained poorly for tyrosinated α-tubulin (tyr-tubulin) and depolymerized relatively slowly in the presence of 2 μg/ml nocodazole ($t_{1/2}$ approx. 130 min), while the other domain stained strongly for tyr-tubulin and depolymerized relatively rapidly in the presence of 2 μg/ml nocodazole ($t_{1/2}$ approx. 3.5 min) (Baas and Black, 1990; Baas et al., 1991). The tyr-tubulin-rich domain was situated at the plus-end of the tyr-tubulin-poor domain, and the transition between these domains was relatively abrupt. We suggested that the tyr-tubulin-rich domain assembles locally within the axon by elongation from the plus-end of the tyr-tubulin-poor domain, and that the tyr-tubulin-poor domains represent the principal and perhaps only long-lived MT nucleating structures in the axon. Subsequent support for this view has been provided by Baas and Ahmad (1992) in experiments that examined MT regrowth in axons during recovery after treatment with nocodazole.

These previous studies used immunoelectron microscopy to visualize composite MTs. This approach revealed striking images of the transition between the two domains of composite MTs (Baas and Black, 1990), and serial reconstruction has permitted analyses along short lengths of these polymers (Baas and Ahmad, 1992). However, even with serial reconstruction, electron microscopy is limited in the number of MTs that can be analysed and the lengths over

which these polymers can be traced. To evaluate more completely the properties of the tyr-tubulin-rich and tyr-tubulin-poor domains of composite MTs, we have developed a preparation that permits visualization of individual axonal MTs over lengths that can exceed 100 μm, using conventional immunofluorescence procedures and epifluorescence microscopy. Using this preparation, we have applied digital image processing and analysis techniques to quantitatively analyse the relative content of tyr-tubulin and acetylated α-tubulin (Ac-tubulin) along single MTs. Our results confirm the composite nature of axonal MTs and suggest novel aspects to the assembly dynamics of MTs in axons.

MATERIALS AND METHODS

Cell culture

Rat sympathetic neurons were grown on glass coverslips coated with poly-lysine and laminin, using slight modifications of the procedure of Higgins et al. (1991), as described by Brown et al., (1992). All of the studies presented here were performed on cultures that varied between 17 and 48 hours in age from the time of plating. By this time, most of the neurons had extended one or more axons and no dendrites.

Immunofluorescence procedures

Prior to fixation, cells were extracted under conditions that stabilize existing MTs and remove unassembled tubulin, using one of two procedures. For procedure 1, neurons were rinsed once with PBS, once with PHEM (60 mM PIPES, 25 mM HEPES, 10 mM EGTA, 2 mM $MgCl_2$, pH 6.9; Schliwa and van Blerkom, 1981), and then extracted for 5 minutes in PHEM containing 1% saponin (Sigma Chemical Co., St. Louis, MO, prepared from Gypsophila sp.), 10 μM taxol (a gift from Dr Matthew Suffness of the National Cancer Institute) and 0.1% dimethyl sulfoxide (Sigma). The purpose of adding dimethyl sulfoxide was to aid dissolution of the taxol. The extraction solution also contained a mixture of protease inhibitors (0.2 trypsin inhibitory units/ml of aprotinin, and 10 μg/ml each of leupeptin, chymostatin and antipain). For procedure 2, cells were rinsed with PBS and PHEM as above and then extracted for 5 minutes with PHEM containing 10 μM taxol, protease inhibitors, 0.1% dimethyl sulfoxide and either 0.2% Triton X-100 (Sigma) or 0.5% Triton X-100 + 0.2 M NaCl.

Extracted cells were then fixed either by immersion in methanol at −20°C for 6 minutes or with 2% paraformaldehyde + 0.05% glutaraldehyde at room temperature for 10 minutes as described by Brown et al. (1992). Methanol-fixed cells were re-hydrated with PBS, treated with blocking solution for 10 minutes and then incubated with primary antibody (see below). The blocking solution consisted of 4% normal goat serum in PBS or a mixture of 2% normal goat serum and 2% normal donkey serum in PBS. The aldehyde-fixed cells were rinsed with PBS and then, for saponin-extracted cells only, treated with 0.1% Triton X-100 in PBS for 15 minutes. Subsequently, the dishes were rinsed with PBS, treated with three 5 minute changes of sodium borohydride (Sigma, 10 mg/ml in a 1:1 mixture of PBS and methanol), rinsed with PBS again and then treated with blocking solution (see above).

The cells were then double-stained according to one of the following protocols. All antibodies were diluted in blocking solution and then clarified prior to use by centrifugation at 200,000 ***g*** for 10 minutes in a Beckman TL-100 ultracentrifuge (Beckman Instruments Inc., Palo Alto, CA). All secondary antibodies were purchased from Jackson Immunoresearch Laboratories Inc., West Grove, PA (AffiniPure grade, pre-adsorbed for minimum cross-reactivity). For some experiments, the cells were incubated simultaneously with a mouse monoclonal antibody against β-tubulin (Amersham Corporation, Arlington Heights, IL; Blose et al., 1984) and a rat monoclonal antibody against tyrosinated α-tubulin (tyr-tubulin) (YL1/2, Accurate Chemical and Scientific Corporation, Westbury, NY; Kilmartin et al., 1982; Wehland and Willingham, 1983; Wehland et al., 1983) exactly as described by Brown et al. (1992). In other experiments, the cells were stained by either simultaneous or sequential incubation with the mouse monoclonal antibody against β-tubulin and a rabbit polyclonal antibody specific for tyr-tubulin (generously provided by Dr Chloe Bulinski, Columbia University, New York, NY). In experiments using sequential incubations with primary antibody, the cells were incubated first with the anti-β-tubulin antibody, rinsed once with blocking solution and then incubated with the anti-tyr-tubulin antibody. The β-tubulin antibody was used at a dilution of 1:200, and the rabbit tyr-tubulin antibody was used at a dilution of 1:3200. After incubation with the primary antibodies, the cells were rinsed extensively with PBS, reblocked, and then incubated with a mixture of secondary antibodies containing FITC-conjugated goat anti-mouse antibody, at a dilution of 1:100, and Texas Red-conjugated donkey anti-rabbit antibody, at a dilution of 1:400 (both obtained from Jackson Immunoresearch). Other cells were double-stained for acetylated α-tubulin (Ac-tubulin) and tyr-tubulin by sequential incubation with a mouse monoclonal antibody specific for Ac-tubulin (6-11B-1, generously provided by Dr Giani Piperno, Rockefeller University, New York, NY; Piperno and Fuller, 1985) and then the rabbit polyclonal antibody against tyr-tubulin (see above). The antibody against Ac-tubulin was provided as a culture supernatant and was used undiluted. After incubation with the primary antibodies the cells were rinsed extensively with PBS, reblocked, and then incubated with the same secondary antibody mixture as described above. For all experiments, cells were rinsed extensively with PBS after incubation with secondary antibody and then mounted in 50% (w/v) glycerol containing 10 mg/ml *n*-propyl gallate (Sigma).

Image acquisition

Cells were observed by differential interference contrast (DIC) or epifluorescence microscopy using a Zeiss Axiovert 35 inverted microscope (Carl Zeiss, Inc., Thornwood, NY). For epifluorescence microscopy, the cells were illuminated with a 100 W mercury arc lamp and observed using fluorescein (Zeiss filter set #10) and rhodamine (Zeiss filter set #14) filter sets. A heat-absorbing colored glass filter (BG40) was inserted into the light path between the light source and the filter block. For 35 mm photography, cells were photographed using TMAX 400 film (Eastman Kodak Co., Rochester, NY; pushed to 800 ASA in the development). For quantitative analyses, images were captured using a CH250 cooled CCD camera (Photometrics Ltd., Tucson, AZ) equipped with a Thompson 7883 CCD chip. The array size of the CCD chip was 384 × 576 and the readout rate was 500 kHz. The temperature of the chip was maintained at about −44°C. Image acquisition was performed on an Apple Macintosh IIfx computer using a Nu200 camera controller board and the BDS-Image processing and analysis software package (Biological Detection Systems, Pittsburgh, PA). Illumination of the sample was controlled using a Uniblitz® electronic shutter (Vincent Associates, Rochester, NY), which was operated automatically from the BDS-Image software using a MAC 2000 Communications Interface Module (Ludl Electronic Products Ltd., Hawthorne, NY).

Images were acquired using the full usable area of the CCD chip, which measured 382 × 576 pixels, and stored in full 12-bit format on 650 megabyte magneto-optical disks using a Pinnacle REO-650 removable erasable optical disk drive (Pinnacle Micro Inc., Irvine, CA). Prior to capturing a series of images, an instan-

taneous readout of the bias voltage offset on the chip was saved and subsequently subtracted from each exposed image. Dark current (0.133 analog-to-digital units/second) was not significant for the exposure times used in these studies. The magnification of the CCD images was calibrated using a stage micrometer. Image processing and analysis was performed using the BDS-Image software and application programs written in this laboratory using the BDS-Image programming language. For maximum precision, all measurements of fluorescence intensity were performed on the 12-bit images. For presentation, monochrome images were scaled to 8-bits for display and photographed from the computer screen using TMAX 100 film (Eastman Kodak) and a 35 mm camera equipped with a macro lens. Photographs of color images were obtained by an electronic imaging process at a local professional photographic laboratory (Quaker Photo, Philadelphia, PA).

Ratio imaging

CCD images acquired using a 100×/1.3 NA Plan-neofluar oil-immersion objective were registered to within half a pixel by shifting each fluorescein image horizontally and vertically to achieve maximum overlap with the corresponding Texas Red image. Images were flat-field corrected (Brown et al., 1992) and then corrected for background by subtracting the mean background pixel intensity for the entire image from each pixel in that image and then setting any negative pixel values to zero. Each pixel in the corrected image of the tyr-tubulin fluorescence was then divided by the corresponding pixel in the corrected image of the β-tubulin fluorescence. The resulting ratio images were displayed using a pseudocolor map in which the magnitude of the ratio for each pixel was represented by the color hue. The spectrum of hues varied from violet (lowest ratio) to red (highest ratio), as shown in Fig. 5.

Quantitative analysis using a segmented mask

For quantitative analyses, cultures were double-stained for tyr-tubulin and β-tubulin or for tyr-tubulin and Ac-tubulin. CCD images of the stained cells were acquired using a 100×/1.3 NA Plan-neofluar oil-immersion objective. To quantify fluorescence intensity along the length of an individual MT, we used image processing techniques to generate a mask of the MT based on the β-tubulin image (for cells double-stained for tyr-tubulin and β-tubulin, see Fig. 7) or based on the sum of the tyr-tubulin and Ac-tubulin images (for cells double-stained for tyr-tubulin and Ac-tubulin, see Fig. 9). The techniques used to produce the mask were identical to those described by Brown et al. (1992) for quantitative analysis of fluorescence intensity along individual axons. Using the procedures described by Brown et al. (1992) to evaluate the efficacy of the masking procedure, we determined that ≥90% of the total MT fluorescence was contained within the mask. After generating the mask, it was divided into 0.9 μm-long segments and then overlaid on the original Texas Red and fluorescein images. This allowed us to define segments in the fluorescence images that corresponded to the segments in the mask. To correct for background fluorescence in each image, an average background pixel intensity was calculated for each segment and then subtracted from each pixel within that segment. Then, the total fluorescence intensity for the segments in each image were calculated by summing the corrected intensities of the pixels within each segment (see Figs 7 and 9). Segments that contained fluorescent debris were omitted from our analyses. In the case of cultures double-stained for tyr-tubulin and β-tubulin, a fluorescence ratio was also computed for each segment by dividing the total intensity for each segment in the image of the tyr-tubulin fluorescence by the total intensity for the corresponding segment in the image of the β-tubulin fluorescence (see Fig. 7). The above procedures have been incorporated into a single, interactive application program written in the BDS-Image programming language. A synopsis of these procedures is presented by Brown et al. (1992), and a more detailed description will be provided upon request.

RESULTS

Visualization of individual axonal MTs by immunofluorescence microscopy

Fig. 1 shows images of sympathetic neurons that were extracted with either saponin or Triton X-100 and then stained to reveal MTs. We have shown previously that the staining under these conditions is due specifically to tubulin in MTs (Brown et al., 1992). In neurons extracted with saponin (Fig. 1A), staining for MTs extends throughout the cell body and the axon but there is little indication of individual polymers. The inability to resolve the signal from individual axonal MTs is a consequence of the relatively tight packing of the MTs in the axon. A very different image is obtained when these neurons are extracted with Triton X-100 (Figs 1B and 2). Under these conditions, we observe many long, uniform tubulin-containing structures that appear to be individual MTs (see below). This suggests that Triton X-100 causes a general loosening of the MT array of the axon, with what appear to be individual MTs separating from each other for variable distances along their lengths. We call this phenomenon fraying, and it is most extensive in the distal 100-200 μm of the axon, where the MT array unravels over long distances.

Fig. 2 shows a higher magnification view of MT fraying along an axon extracted with Triton X-100. In the proximal axon and axon shaft, there is only a slight unravelling of the MT array (Fig. 2A, C); individual MTs can be followed for only a few microns, and MT ends are rarely encountered. In the region of the distal axon (Fig. 2E), within 100-200 μm of the growth cone, the extent of fraying is much greater than in the axon shaft; many MT ends are apparent and individual MTs can frequently be traced for ≥20 μm.

The extent of fraying caused by Triton X-100 varied considerably from one neuron to another within individual experiments and also between experiments. In some experiments, little fraying was observed with Triton X-100, but including 0.2 M NaCl in the extraction solution greatly enhanced the extent and reproducibility of the fraying (Fig. 1C). Furthermore, extraction with Triton X-100 + 0.2 M NaCl often caused considerable fraying along the entire axon, although the most extensive fraying still typically occurred in the distal region. In these more extensively frayed preparations, individual MTs could frequently be traced for several tens of micrometres within the axon shaft, and for distances of 50 μm or more in the distal region of the axon (see Figs 3B and 4). Extraction with Triton X-100 + NaCl also frequently caused MTs to separate completely from the axon, thereby permitting visualization of both ends of these polymers. The lengths of these isolated polymers varied from about 10 μm to about 130 μm. We do not know whether the length of these MTs reflects their actual length in the axon prior to extraction or whether these polymers represent fragments of longer MTs that broke during processing.

As indicated above, many of the β-tubulin-containing structures revealed in the frayed preparations appear to represent individual MTs. This conclusion is supported by the close resemblance in intensity and diameter between these structures and individual MTs in non-neuronal cells that were present in the same cultures (see Fig. 3A,B). If these structures do correspond to individual MTs, then they should stain uniformly along their length for β-tubulin. Analyses that used the segmented mask procedure (see Materials and methods) to quantify β-tubulin fluorescence in consecutive 0.9 μm segments of these tubulin-containing structures confirmed this expectation (see Fig. 7). We computed the mean and standard deviation of the fluorescence intensity for all of the segments comprising each tubulin-containing structure that we analysed. These structures ranged in length from 30 to 128 μm. For each structure, the standard deviation was ≤16% of the mean (average = 10%, range 7-16%, n = 10). The low value of the standard deviations relative to their respective means demonstrates the uniformity of the β-tubulin staining along these structures, and this supports the conclusion that they represent individual MTs.

These observations indicate that extraction with Triton X-100, or with Triton X-100 + NaCl, causes the axonal MTs to unravel so that individual MTs can be visualized using conventional immunofluorescence procedures and epifluorescence microscopy. In the vast majority of cases, these MTs can be traced for only part of their length. While the actual length of MTs revealed in the frayed preparations varied considerably from one MT to another, lengths of several tens of micrometres were frequently encountered, and we were able to trace individual MTs for lengths in excess of 100 μm in a limited number of cases (for example, see Fig. 7A). In the distal region of the axon, frayed MTs could typically be traced to their most distal end (relative to the cell body), which corresponds to their plus-end. We have not been able to identify with confidence the minus-ends of these MTs because they are situated more proximally in the axon shaft, where the extent of fraying is insufficient to reveal them.

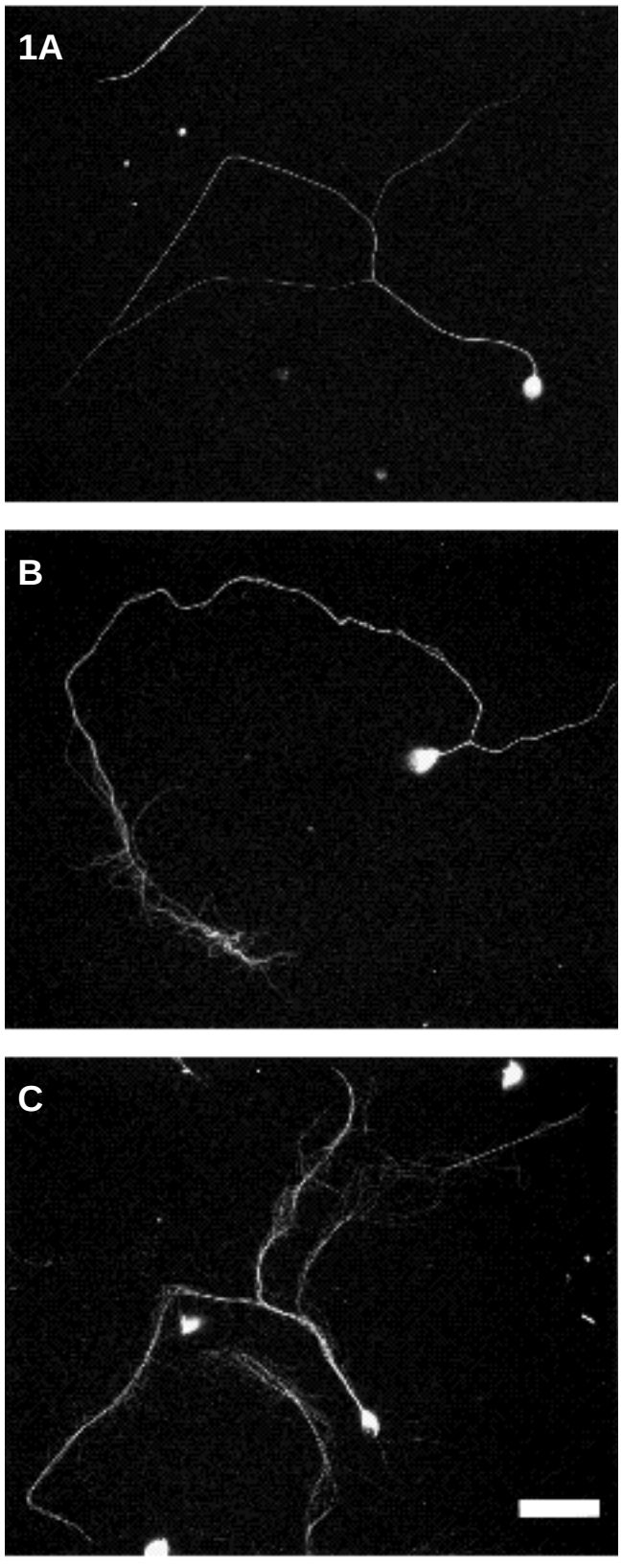

Fig. 1. Effect of extraction procedure on the MT array of the axon. MT staining patterns in cultured neurons extracted with a MT-stabilizing solution containing 1% saponin (A), 0.2% Triton X-100 (B) or 0.5% Triton X-100 + 0.2 M NaCl (C). The neurons depicted in A and B were fixed by immersion in cold methanol, and the neuron depicted in C was fixed with the paraformaldehyde/glutaraldehyde mixture. In all cases, MTs were revealed by staining with the antibody specific for β-tubulin. Bar, 50 μm.

Fig. 2. MT fraying along the length of an axon. Contiguous fields are shown, depicting an entire axon from the cell body to the growth cone (these are high magnification views of the cell shown in Fig. 1 B). This neuron was extracted with 0.2% Triton X-100, fixed by immersion in cold methanol, and then double-stained to reveal total MTs (A, C, E) and tyrosinated MTs (B, D, F) by simultaneous incubation with a mouse monoclonal antibody to β-tubulin and a rat monoclonal antibody to tyr-tubulin, respectively. All of the images that were stained for β-tubulin were obtained with the same exposure time at the microscope and also with the same exposure time at the enlarger.Similarly, all of the images that were stained for tyr-tubulin were obtained with the same exposure time at the microscope and the also with the same exposure time at the enlarger. The arrows indicate transitions between tyr-tubulin-rich and tyr-tubulin-poor domains of composite MTs (see text). Bar, 20 μm.

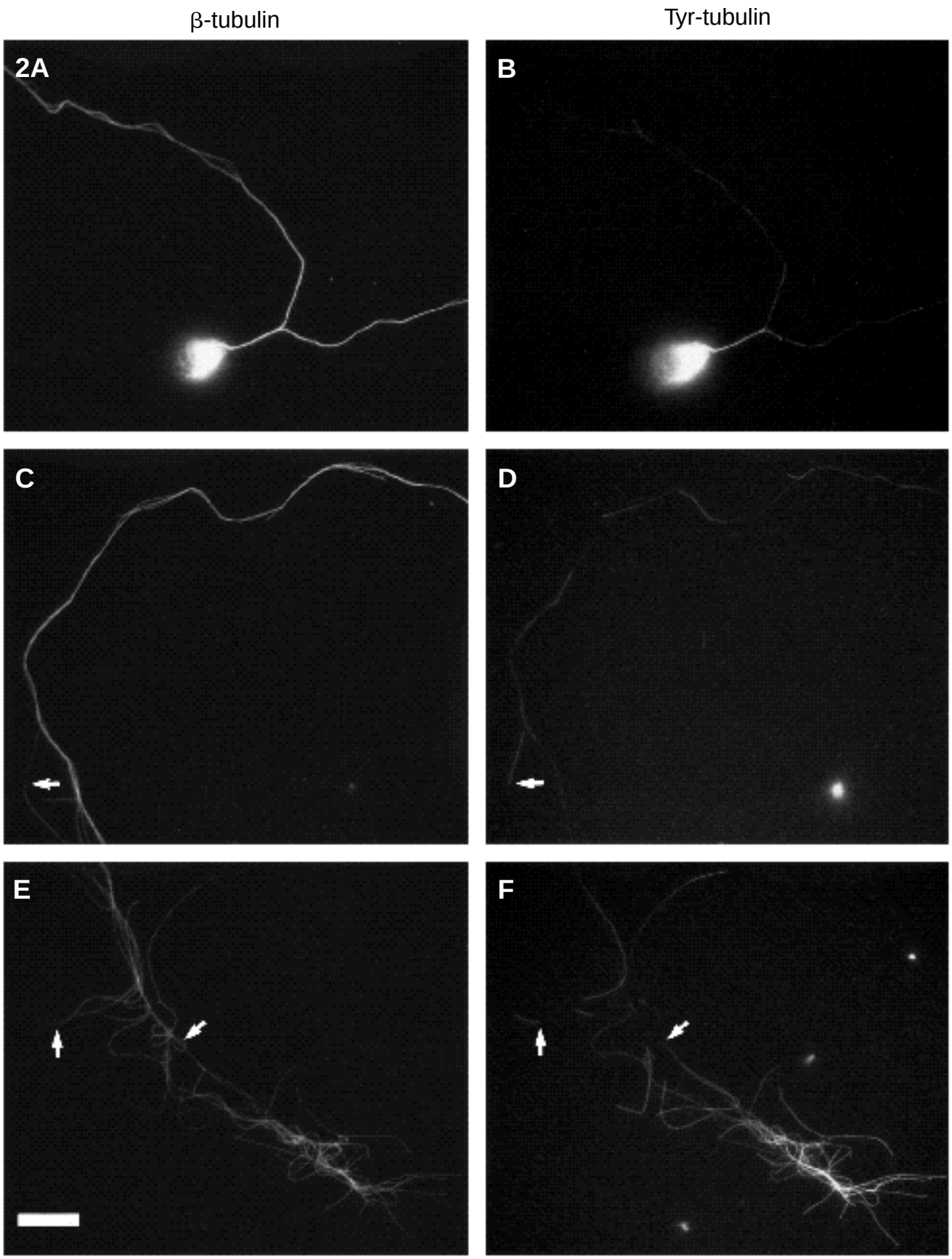
β-tubulin
Tyr-tubulin
2A
B
C
D
E
F

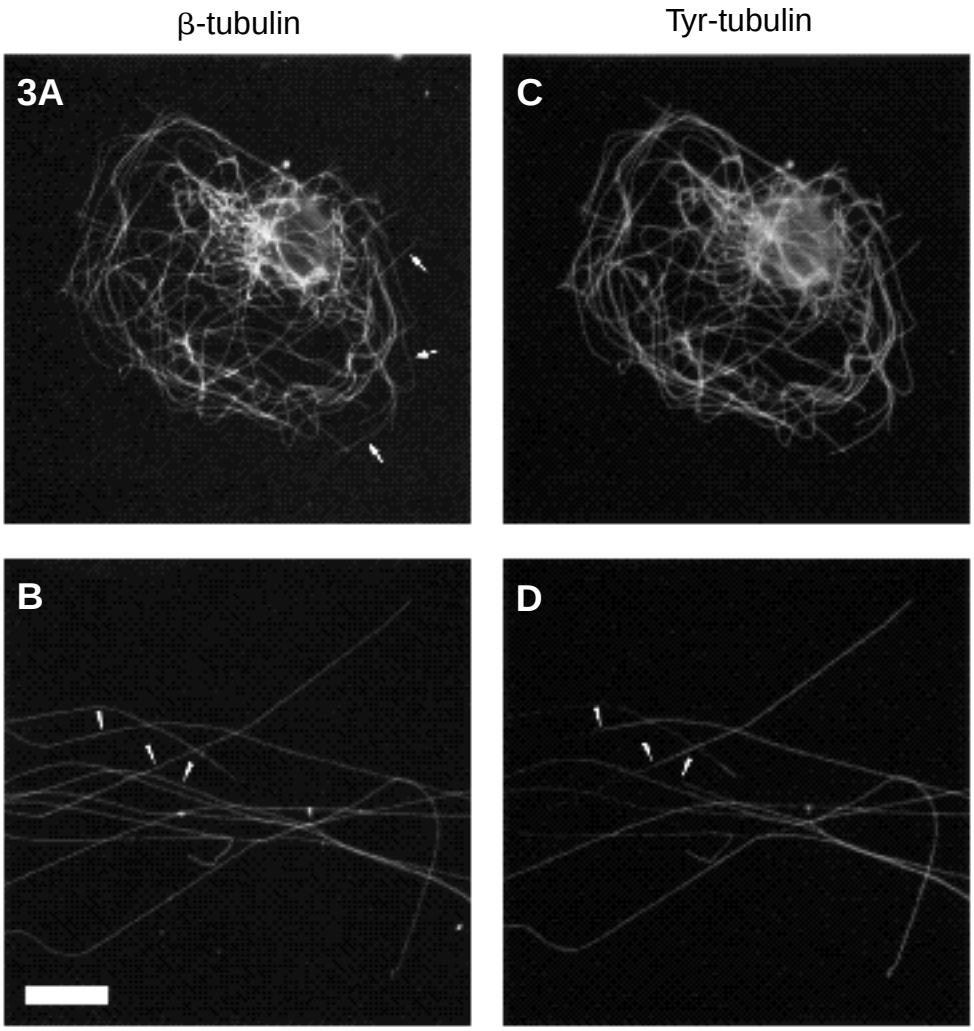

Fig. 3. Immunofluorescence images of frayed axonal MTs closely resemble those of individual MTs in non-neuronal cells. Cells extracted with 0.5% Triton X-100 + 0.2 M NaCl were fixed with the paraformaldehyde/glutaraldehyde mix and then double-stained for β-tubulin and tyr-tubulin. (A) and (C) show images of the β-tubulin and tyr-tubulin fluorescence, respectively, for a typical non-neuronal cell. (B) and (D) show images of the β-tubulin and tyr-tubulin fluorescence, respectively, for a frayed axon. The axon shown in B and D is orientated so that the cell body and proximal axon are towards the left and the growth cone and distal axon are towards the right. Note that individual frayed MTs in the axons (B) stained for β-tubulin with similar intensity as individual MTs in the non-neuronal cells (see arrows in A). Many of the MTs in the frayed preparations also stained for tyr-tubulin (D), and the intensity of this staining was also similar to that of individual MTs in non-neuronal cells (C). However, unlike the non-neuronal MTs, many of the axonal MTs stained for tyr-tubulin over only part of their length; the arrowheads in B and D indicate transitions between the tyr-tubulin-rich and tyr-tubulin-poor domains of these composite MTs (see text). Bar, 11 μm.

Regional differences in staining of MTs for tyr-tubulin

We have shown previously, using unfrayed preparations, that staining for tyrosinated α-tubulin (tyr-tubulin) in polymers varies along the axon, such that staining is much brighter in the proximal and distal regions of the axon than along the axon shaft (Brown et al., 1992). Using the frayed preparation, we have examined the nature of this regional variation at the level of individual MTs. Fig. 2 shows images along the length of an axon extracted with Triton X-100 and then double-stained for β-tubulin and tyr-tubulin. The β-tubulin staining is relatively uniform along the length of the axon, whereas the staining for tyr-tubulin is characteristically bright proximally and distally but dim along the axon shaft. Note that all of the MT polymer discernable stains brightly for tyr-tubulin in the distal 30-50 μm of the axon (Fig.2 E, F), whereas only discrete MT segments stain for tyr-tubulin within the axon shaft, with much of the MT polymer appearing either unstained or poorly stained (Fig.2C, D; see also Fig. 4). The situation in the proximal axon (defined as the first 40 μm of the axon; see Brown et al., 1992) is more difficult to evaluate because of the limited fraying that occurs in this region. However, whenever frayed MTs were observed in this region, they stained strongly for tyr-tubulin (data not shown). In addition, the tyr-tubulin-rich MTs in the distal 30-50 μm of the axon stained more brightly than the tyr-tubulin-rich MTs in

Fig. 4. Composite MTs revealed by staining for tyr-tubulin. Cells extracted with 0.2% Triton X-100 (C, D) or 0.5% Triton X-100 + 0.2 M NaCl (A, B, E, F) were fixed by immersion in cold methanol (C, D) or with the paraformaldehyde/glutaraldehyde mixture (A, B, E, F), and then double-stained for tyr-tubulin and β-tubulin. The images in C and D were obtained by simultaneous incubation with the mouse monoclonal antibody to β-tubulin and the rat monoclonal antibody to tyr-tubulin. The other images (A, B, E, F) were obtained by sequential incubation with the mouse monoclonal antibody to β-tubulin followed by the rabbit polyclonal antibody against tyr-tubulin. Each axon in this figure is orientated so that the cell body and proximal axon are towards the left and the growth cone and distal axon are towards the right. The arrowheads mark transitions between the tyr-tubulin-poor and tyr-tubulin-rich domains of individual composite MTs. Some of the MTs that appear to be composite in these images are not marked because of ambiguity in tracing them due to overlap with other MTs. A-D show composite MTs in the region of the growth cone and E and F show composite MTs within an axon shaft. Bar, 10 μm.

the axon shaft. This can be appreciated by comparing the brightness of the tyr-tubulin containing MT segments in the axon shaft with the tyr-tubulin containing polymer in the distal axon (Fig. 2). Thus, the tyr-tubulin-rich MT polymer in the distal region of the axon contains more tyr-tubulin than the tyr-tubulin-rich polymer in the axon shaft.

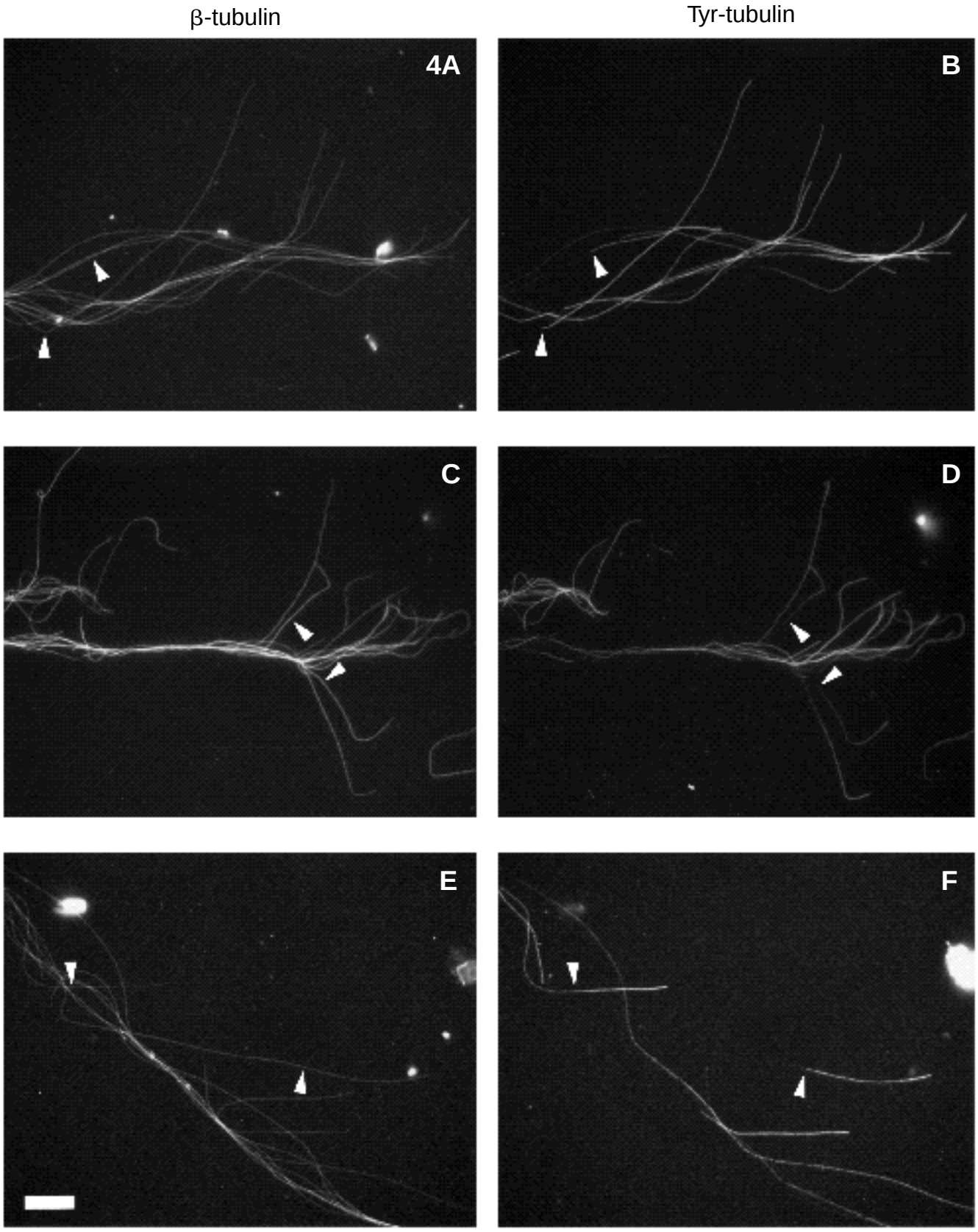

Visualization of tyr-tubulin-rich and tyr-tubulin-poor domains along individual MTs

In a previous study using immunoelectron microscopy, we have shown that individual MTs of the axon consist of distinct domains that differ in their content of tyr-tubulin (Baas and Black, 1990). In the present study, we have confirmed and extended these observations using the frayed preparation. Figs 2, 3 and 4 show images of frayed preparations double-stained for β-tubulin and tyr-tubulin. All of the individual MTs apparent in the frayed preparations stained uniformly for β-tubulin along their length. In contrast, all MTs did not stain uniformly along their length for tyr-tubulin. Specifically, many MTs exhibited a single and relatively abrupt transition from a domain that stained poorly for tyr-tubulin to a domain that stained strongly for tyr-tubulin (Figs 2, 3 and 4). We refer to these MTs as composite because they consist of distinct domains that differ in their content of post-translationally modified tubulin subunits. Such composite MTs were never observed in the non-neuronal cells that were occasionally present in the cultures (see Fig. 3 A,C). In all but one case, composite MT profiles consisted of a single tyr-tubulin-poor domain and a single tyr-tubulin-rich domain, irrespective of the total length of the MT. In this regard, the longest composite MT observed was 128 μm (see Fig. 7 A,B). This MT became separated from the axon during extraction so that both of its ends were apparent; its tyr-tubulin-rich domain was 61 μm long, and its tyr-tubulin-poor domain was 67 μm. The one exception was a 47 μm-long MT for which both ends were visible. This MT consisted of two tyr-tubulin-rich domains, one at each end of the MT, separated by a tyr-tubulin-poor domain.

Composite MTs were more difficult to detect in the axon shaft than in the distal region of the axon because of the more limited degree of fraying in this region of the neuron. Generally, tyr-tubulin-rich MT segments in the axon shaft appeared as relatively bright streaks (about 5-50 μm long) that could not be resolved from neighboring MTs (Fig. 2 C, D). In the small number of cases where these segments frayed apart from the axon, they appeared to be contiguous with more proximal tyr-tubulin-poor segments. In this regard, Fig. 4 E, F shows several examples of transitions between tyr-tubulin-rich and tyr-tubulin-poor domains of individual MTs in the axon shaft.

The following evidence indicates that the tyr-tubulin-rich domains at the ends of composite MTs exist in intact axons and are not the result of post-lysis assembly of tyr-tubulin during extraction. Specifically, observation by phase contrast microscopy indicates that extraction of axons with 0.2% or 0.5% Triton X-100 is extremely rapid; the phase density of the axon declines very rapidly during the first few seconds of extraction, and the axons are no longer visible after 15-30 seconds. During this period, the concentration of free tubulin available for assembly declines by many orders of magnitude as it diffuses out of the cells into the extraction solution (the unassembled tubulin from 10-30 cells/culture is diluted into 2 ml of extraction solution). As a result, there is only a limited time period for any post-lysis assembly to occur. The assembly rates of pure tubulin or tubulin in cell extracts have been measured under a variety of conditions, with many measurements falling in the range of 1-3 μm/min for tubulin concentrations of 1-2 mg/ml (see Kristoferson et al., 1986; Gard and Kirschner, 1987; Walker et al., 1988). Assuming that post-lysis assembly occurs for the first minute of the extraction, and that this assembly occurs at a rate of 3 μm/min, then 3 μm of MT would form during the extraction period. Our measurements of the lengths of the tyr-tubulin-rich domains indicate that they are quite variable among the composite MTs detected in any given culture (Fig. 6). However, all of the tyr-tubulin-rich domains that we observed were longer than 3 μm, and many were longer than 30 μm. These considerations suggest that post-lysis assembly contributes minimally to the tyr-tubulin-rich MT domains seen in the frayed preparations.

To evaluate further the contribution of post-lysis assembly, cells were extracted with Triton X-100 and then

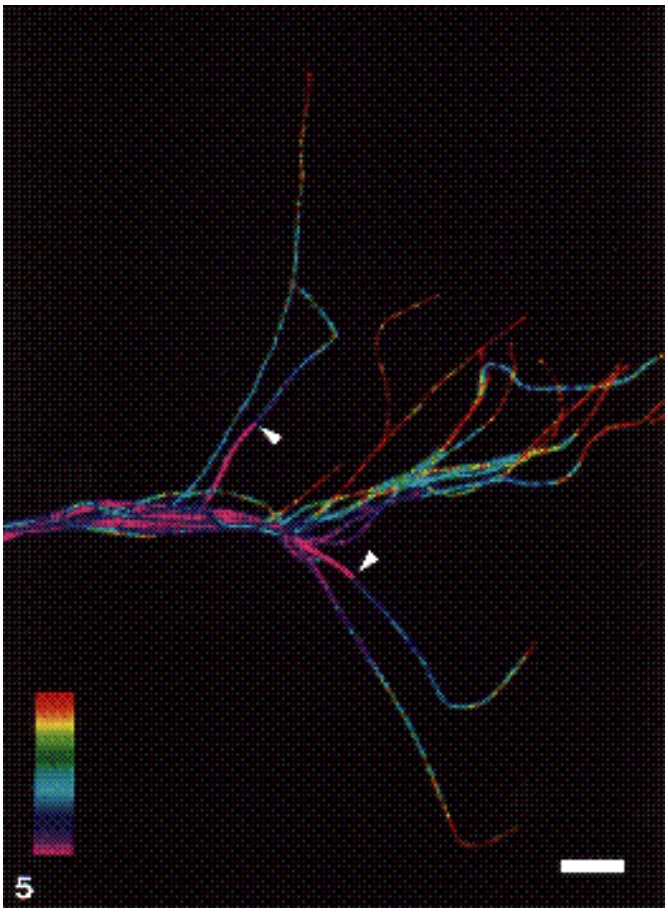

Fig. 5. Pseudocolor ratio imaging of composite MTs in the region of a frayed growth cone. CCD images of the growth cone shown in Fig. 4C, D were obtained as described in Materials and Methods. To obtain the pixel-by-pixel ratio image, the CCD images were edited to remove extraneous objects and then each pixel in the tyr-tubulin-stained image was divided by the corresponding pixel in the β-tubulin-stained image. The color key indicates the spectrum of colors used to represent the magnitude of the ratio. High ratios are represented by the color red and low ratios are represented by the color violet. Each arrowhead marks an abrupt transition between the tyr-tubulin-poor and tyr-tubulin-rich domains of a composite MT. Bar, 8 μm.

double-stained with antibodies against tyr-tubulin and detyrosinated tubulin. It has been established that unassembled tubulin in cells is tyrosinated, and that this tubulin is converted to detyrosinated tubulin after it assembles into MTs in a time-dependent manner (Gunderson et al., 1987). Because it is unlikely that tyr-tubulin could both assemble and be detyrosinated during the extraction procedure, any MT segments that form post-lysis should stain exclusively for tyr-tubulin. We observed that all of the MT segments that stained brightly for tyr-tubulin also contained detectable levels of detyrosinated tubulin all along their entire length (data not shown; see also Baas et al., 1991). Similar observations were also obtained in experiments in which frayed MTs were double-stained for tyr-tubulin and Ac-tubulin (see Figs 8 and 9). Finally, it is possible that the taxol present in the extraction solution may induce post-lysis assembly during the early stages of extraction. To test this possibility, cells were extracted with 0.2% Triton X-100 for 30 seconds before adding taxol to the extraction solution. We observed no obvious difference in the pattern of staining for tyr-tubulin in these cells compared with cells that were extracted continuously in the presence of taxol (data not shown). These observations are not consistent with significant post-lysis assembly of MT polymer.

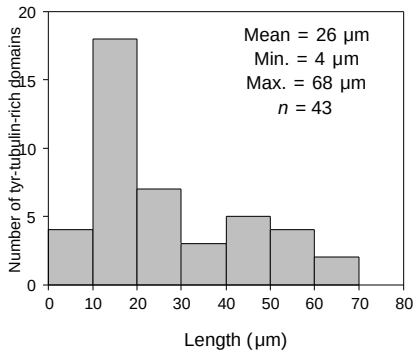

Fig. 6. Histogram showing the distribution of lengths for the tyr-tubulin-rich domains of composite MTs. The data shown were all obtained from a single frayed preparation. To minimize bias in our selection of composite MTs for measurement, we measured the tyr-tubulin-rich domains of all of the composite MTs that we encountered which could be traced unambiguously from the transition to the end of the tyr-tubulin-rich domain.

In our original study of composite MTs (Baas and Black, 1990), the tyr-tubulin-rich domain was always observed at the plus-end of the tyr-tubulin-poor domain, though the total number of transitions that we were able to locate was only 21. In the present study, we have been able to extend these

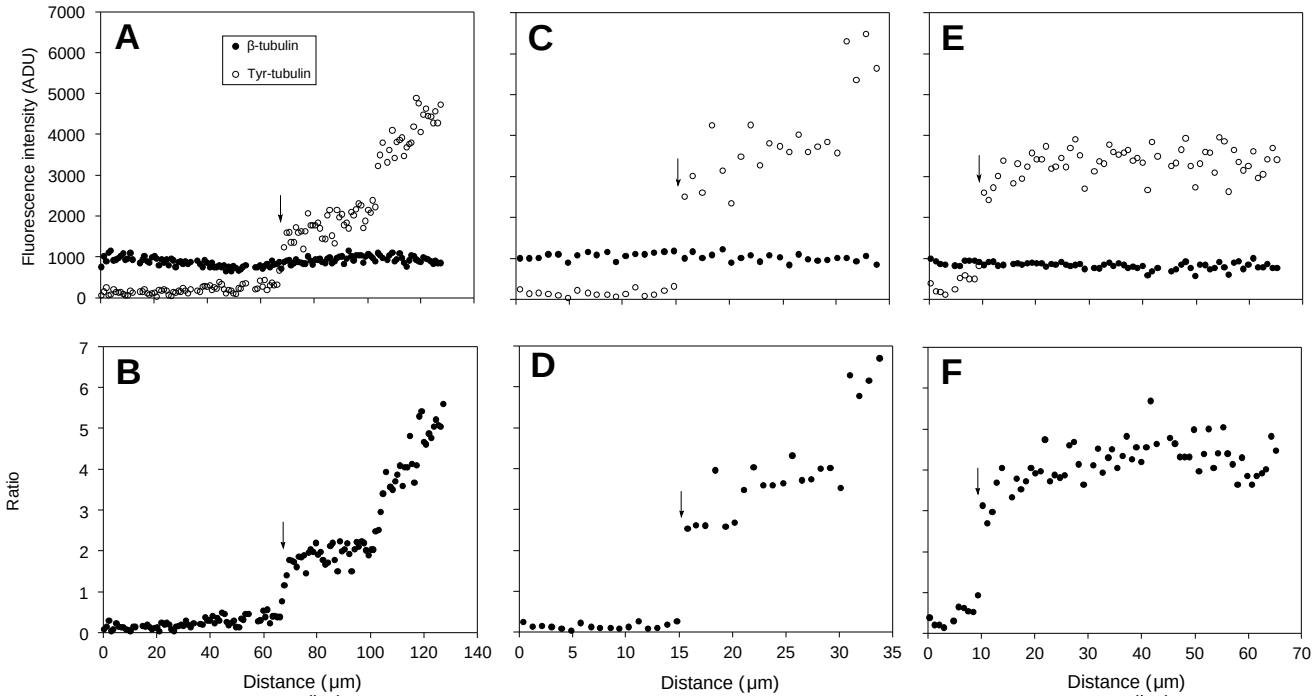

Fig. 7. Quantitative analyses of tyr-tubulin and β-tubulin staining intensity along the length of individual composite MTs. (A) and (B) show data for the entire length of a single MT that had separated completely from the axon so that it could be traced unambiguously from its proximal (minus) end to its distal (plus) end. (C-F) show data for the distal portions of two other MTs which could be traced unambiguously to their distal (plus) ends but could not be traced unambiguously to their proximal (minus) ends because of overlap with other MTs. The MTs were fixed with the paraformaldehyde/glutaraldehyde mixture and stained by sequential incubation with the mouse monoclonal antibody to β-tubulin followed by the rabbit polyclonal antibody against tyr-tubulin. The fluorescence intensities due to β-tubulin and tyr-tubulin were quantified in consecutive 0.9 µm-long segments of the MTs using the segmented mask procedure described in Materials and Methods. The upper graphs show the fluorescence intensity values in analog-to-digital units (ADU) for β-tubulin (filled circles) and for tyr-tubulin (open circles) in each segment, plotted against distance along the MT. The lower graphs show the ratio of the tyr-tubulin fluorescence intensity to the β-tubulin fluorescence intensity for each segment. The arrow on each graph marks the transition between the tyr-tubulin-poor and tyr-tubulin-rich domains. Because the fluorescence intensities were measured in arbitrary analog-to-digital units, the magnitude of the ratio in the lower graphs represents a relative measure of the proportion of tubulin that is tyrosinated.

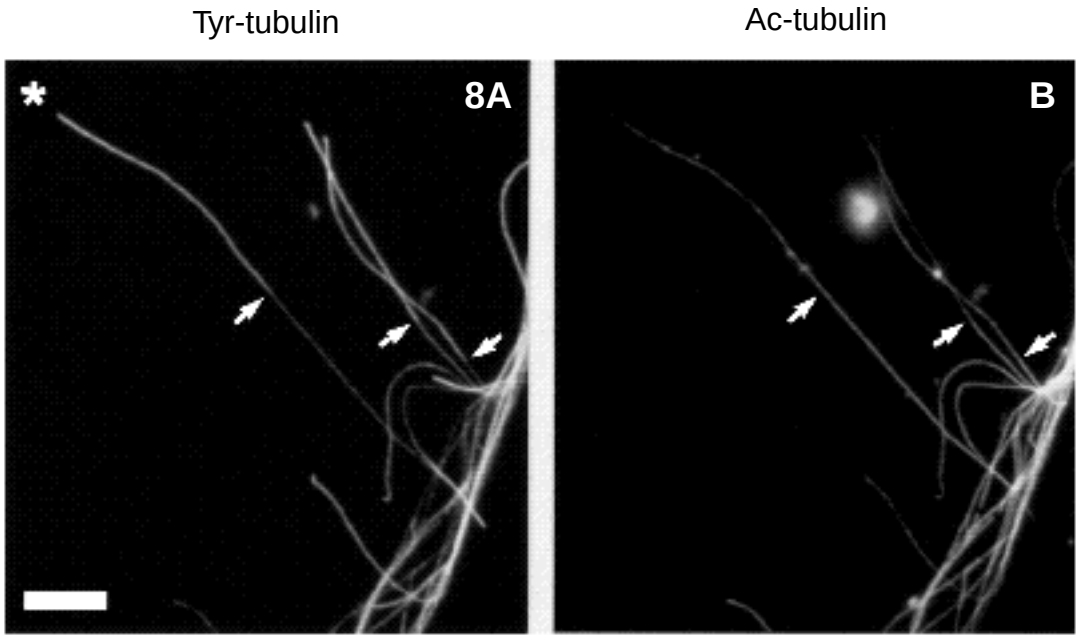

Fig. 8. Composite MTs revealed by staining for Ac-tubulin. Cells extracted with 0.5% Triton X-100 + 0.2 M NaCl were fixed with the paraformaldehyde/glutaraldehyde mixture and then double-stained by sequential incubation with the mouse monoclonal antibody against Ac-tubulin followed by the rabbit polyclonal antibody against tyr-tubulin. CCD images of the tyr-tubulin staining (A) and Ac-tubulin staining (B) are shown. The arrows in each image mark the sites of transition between the tyr-tubulin-poor and tyr-tubulin-rich domains of individual composite MTs. The MT indicated with an asterisk (*) in A was analysed quantitatively using the segmentation procedure (see Fig. 9 A,B). Bar, 11 μm.

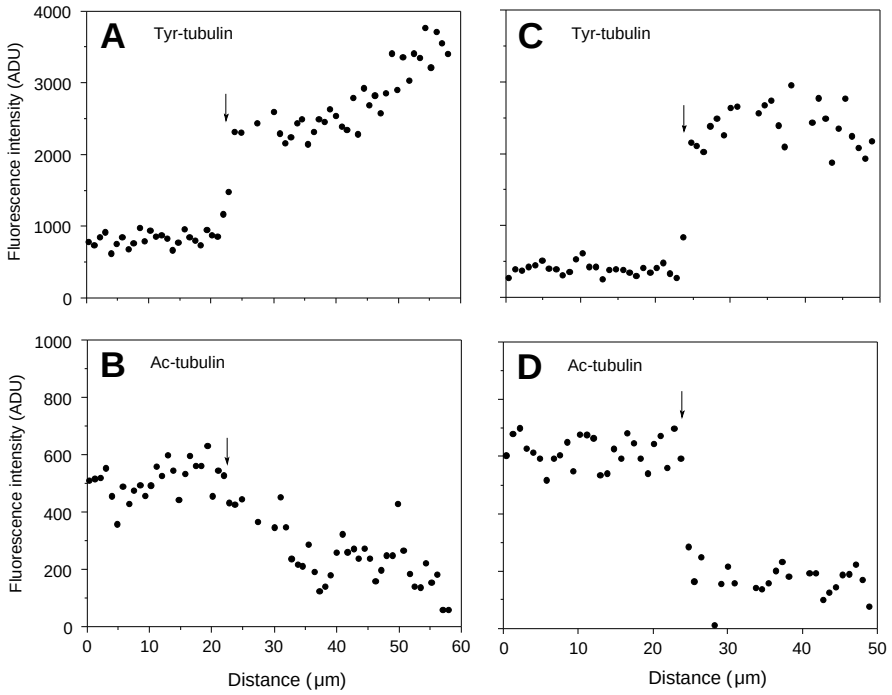

Fig. 9. Quantitative analyses of tyr-tubulin and Ac-tubulin staining intensities along the length of individual composite MTs. Data are shown for the distal portions of two different MTs. Both MTs could be traced unambiguously to their distal (plus) ends but could not be traced unambiguously to their proximal (minus) ends because of overlap with other MTs. The MTs were fixed with the paraformaldehyde/glutaraldehyde mixture and then stained by sequential incubation with the mouse monoclonal antibody to Ac-tubulin followed by the rabbit polyclonal antibody against tyr-tubulin. The fluorescence intensities due to Ac-tubulin and tyr-tubulin were quantified in consecutive 0.9 μm-long segments of the MT using the segmented mask procedure described in the Materials and methods section. The fluorescence intensity values for tyr-tubulin in each segment are plotted against distance along the MT in (A) and (C), and the corresponding values for Ac-tubulin are shown in (B) and (D). The data shown in A and B were obtained from the MT indicated by an asterisk (*) in Fig. 8A. Some of the segments along this MT were omitted from the graphs because they contained fluorescent debris (see Fig. 8 B). The arrow on each graph marks the transition between the tyr-tubulin-poor and tyr-tubulin-rich domains. ADU, analog-to-digital units.

observations because the frayed preparations have allowed us to visualize large numbers of composite MTs. In many of the frayed preparations, we could trace composite MTs all the way to their distal ends and also infer their polarity orientation based on their orientation relative to the cell body (see, for example, Figs 2, 4, 5). In all of these cases, the tyr-tubulin-rich domain extended to the end of the polymer that was most distal relative to the cell body. We have shown previously that MTs in the axons of cultured sympathetic neurons are uniform in polarity orientation, having their plus-ends pointing away from the cell body toward the axon tip (Baas et al., 1991). Thus, the tyr-tubulin-rich domain of composite MTs is situated at the plus-end of the tyr-tubulin-poor domain and extends to the plus-end of the MT.

To visualize the distribution of tyr-tubulin along individual MTs, we performed fluorescence ratio imaging. Fig. 5 shows a ratio image for the frayed axon shown in Fig. 4 C, D. Ratio imaging provided a striking illustration of the relatively abrupt change in the tyr-tubulin content of composite MTs at the transition between the tyr-tubulin-poor and tyr-tubulin-rich domains. In addition, ratio imaging also revealed that the relative content of tyr-tubulin within the tyr-tubulin-rich domain was not constant, but increased progressively from the transition toward the distal end of the MT. To examine this observation more rigorously, we performed quantitative analyses in which digital image processing techniques were used to measure the fluorescence due to β-tubulin and tyr-tubulin in contiguous 0.9 μm segments along the length of individual composite MTs. To obtain a measure of the relative amount of tyr-tubulin along the length of these MTs, we divided the tyr-tubulin fluorescence by the β-tubulin fluorescence for each segment and then graphed the resulting ratio values against distance along the MT. For each segment, the magnitude of the ratio provides a relative measure of the proportion of tyr-tubulin in the polymer contained within that segment.

Fig. 7 shows the results of the quantitative analyses for three different composite MTs. The staining for β-tubulin was uniform along the length of each MT that we analysed, as expected for single MTs (see above). In the tyr-tubulin-poor domain (proximal to the transition), the staining intensity for tyr-tubulin was relatively low and also more or less uniform. At the transition, the staining for tyr-tubulin increased abruptly, forming a tyr-tubulin-rich domain that extended to the distal end of the MT. The transition extended over a variable number of segments (between 1 and 4), which corresponded to a distance of between 0.9 and 3.6 μm. The shapes of the ratio profiles within the tyr-tubulin-rich domains fell into two general categories. For all but one of the MTs analysed (6 out of 7), the proportion of tyr-tubulin increased from the transition towards the distal end of the MT in a complex and non-linear manner. Specifically, the tyr-tubulin content increased abruptly at the transition to reach a plateau of variable length in the proximal part of the tyr-tubulin-rich domain. The plateau was followed by a second abrupt increase in ratio within the tyr-tubulin-rich domain to reach the highest proportion of tyr-tubulin at the distal end of the MT (see Fig. 7 B, D). For the remaining MT (1 out of 7), the tyr-tubulin content also increased abruptly at the transition, but then remained fairly constant throughout the tyr-tubulin rich domain; a second abrupt increase in tyr-tubulin content was not apparent for this MT (Fig. 7F). Comparison of the average ratio in the distal region of the tyr-tubulin-poor domain with the average ratio in the plateau region of the tyr-tubulin-rich domain showed that the relative proportion of tyr-tubulin in the MTs increased by 770 ± 630% (mean ± s.d., range = 220-2400%, n = 7) across the transition.

Visualization of Ac-tubulin-rich and Ac-tubulin-poor domains along individual MTs

Fig. 8 shows images of a frayed preparation double-stained for tyr-tubulin and acetylated α-tubulin (Ac-tubulin). Typical composite MTs, with tyr-tubulin-rich and tyr-tubulin-poor domains, are readily visualized. We found that the distribution of Ac-tubulin between these two domains was somewhat complementary to that of tyr-tubulin. Specifically, the tyr-tubulin-poor domain stained relatively brightly for Ac-tubulin, whereas the tyr-tubulin-rich domain stained relatively poorly for Ac-tubulin. For some MTs (3 out of 4), there was a relatively abrupt decrease in Ac-tubulin staining intensity that corresponded in position to the transition in tyr-tubulin staining intensity (Fig. 9C,D). For these MTs, the Ac-tubulin staining intensity appeared to be fairly constant throughout most of the the tyr-tubulin-rich domain. For the remaining MT (1 out of 4), the Ac-tubulin staining also began to decrease at the transition, but this decrease proceeded more gradually, reaching low levels only in the most distal region of the tyr-tubulin-rich domain (Fig. 9A, B). Comparison of the average staining intensity for Ac-tubulin in the distal region of the tyr-tubulin-poor/Ac-tubulin-rich domain with the average staining intensity for Ac-tubulin in the tyr-tubulin-rich/Ac-tubulin-poor domain showed that the amount of Ac-tubulin in the MTs decreased by 62 ± 11% (mean ± s.d., range = 49-75%, n = 4) across the transition.

DISCUSSION

We have developed a novel preparation, which we term the frayed preparation, that permits visualization of individual axonal MTs using conventional immunofluorescence procedures and epifluorescence microscopy. It is not clear how fraying occurs, and no single aspect of the procedure is, in and of itself, sufficient to cause fraying. For example, fraying is not observed when neurons that are grown on a collagen substrate are extracted under identical conditions (Baas and Black, 1990; Baas et al., 1991). Similarly, fraying is not observed when neurons that are grown on a substrate of poly-lysine and laminin are permeabilized with saponin instead of Triton X-100 (Fig. 1). Rather, fraying appears to depend on a combination of growth and extraction conditions. Whether the specific combination of conditions used in the present studies are unique in causing fraying, or whether other combinations of substrata and extraction conditions can also cause fraying, remains to be determined.

The frayed preparation provides a unique opportunity to visualize individual axonal MTs by light microscopy and offers a much more complete view of axonal MTs than can be obtained by other procedures. For example, electron

microscopy provides rather limited views (of about 1 μm) along the length of individual MTs, and MT ends can only be identified by serial reconstruction. By contrast, individual MT profiles in excess of 50 μm are commonly encountered in frayed preparations (see Figs 3-5), and in many cases one end of these polymers, usually the plus-end, can be identified unambiguously. Furthermore, in a limited number of cases, MTs become separated completely from the axon, permitting visualization of both of their ends. Assuming that the average length of MTs in the axons of cultured sympathetic neurons is approx. 100 μm (Bray and Bunge, 1981), then frayed preparations often reveal half or more of the total length of individual axonal MTs. In the present report, we have used the frayed preparations to expand upon our earlier work on differences in the composition of axonal MTs long their length.

We demonstrated previously that individual axonal MTs are composite, consisting of two distinct domains that differ in their content of tyr-tubulin (Baas and Black, 1990). The present results confirm and extend these observations in several respects. Firstly, double-staining of frayed preparations for tyr-tubulin and β-tubulin revealed many dramatic examples of composite MTs (Figs 3-5). With one exception, all of the composite MT profiles that we observed consisted of two distinct domains, one that stained strongly for tyr-tubulin and one that stained poorly (see Results). The transition between these two domains was relatively abrupt, with an increase in the staining intensity of about 800% in proceeding from the tyr-tubulin-poor domain into the tyr-tubulin-rich domain (see Results). Secondly, in all the cases in which we could adequately evaluate the polarity orientation of these composite MT profiles (see Results), the tyr-tubulin-rich domain always extended from the plus-end of the tyr-tubulin-poor domain to the plus-end of the MT. Thirdly, we found that these two domains also differed in their content of Ac-tubulin (Figs 8 and 9). Specifically, the tyr-tubulin-poor domain was relatively rich in Ac-tubulin, whereas the tyr-tubulin-rich domain was relatively poor in Ac-tubulin. Thus, the relative amounts of Ac-tubulin and tyr-tubulin along the length of the MT varied in a more or less complementary manner.

Previous studies in this laboratory have shown that the tyr-tubulin-rich and tyr-tubulin-poor domains of composite MTs differ in their sensitivity to MT depolymerizing agents (Baas and Black, 1990; Baas et al., 1991). Specifically, the tyr-tubulin-rich polymer depolymerizes rapidly in the presence of 2 μg/ml nocodazole ($t_{1/2} \approx 3.5$ min), whereas the tyr-tubulin-poor polymer depolymerizes much more slowly ($t_{1/2} \approx 130$ min). The rate of loss of MTs in the presence of depolymerizing drugs such as nocodazole is dependent in part on their normal turnover dynamics, with MTs that turn over rapidly depolymerizing faster than MTs that turn over slowly (Cassimeris et al., 1986; Kreis, 1987; Wadsworth and McGrail, 1990). On this basis, we have suggested that the drug-stable (tyr-tubulin-poor) domains of axonal MTs are less dynamic than the drug-labile (tyr-tubulin-rich) domains, and consequently that they turn over more slowly in the axon (Baas and Black, 1990). This interpretation is reinforced by the differences in the tyr-tubulin and Ac-tubulin content of these domains. Several observations indicate that the relative content of tyr-tubulin in MTs varies inversely with polymer age, whereas the relative content of Ac-tubulin in MTs varies directly with age (Bré et al., 1987; Gundersen et al., 1987; Kreis, 1987; Schulze et al., 1987; Sherwin et al., 1987; Webster et al., 1987; Wehland and Weber, 1987; Sherwin and Gull, 1989). As a result, recently assembled MTs contain greater amounts of tyr-tubulin than older, more long-lived MTs, while the converse is true for Ac-tubulin. Thus, the tyr-tubulin-poor/Ac-tubulin-rich domains of composite MTs are older (more long-lived) than the tyr-tubulin-rich/Ac-tubulin-poor domains.

In our original immunoelectron microscopic study on composite axonal MTs, we proposed that each composite MT is composed of a single tyr-tubulin-rich domain continuous with the plus-end of a single tyr-tubulin-poor domain (Baas and Black, 1990). The present immunofluorescence study supports this proposal. Specifically, all but one of the many composite MTs that we observed had a single tyr-tubulin-rich domain directly continuous with the plus-end of a single tyr-tubulin-poor domain. These observations suggest that the plus-end of the tyr-tubulin-poor domain is assembly-competent and that it can nucleate MT assembly within the axon. Recent experiments on the reassembly of MTs in axons after treatment with nocodazole have lent strong support to this hypothesis (Baas and Ahmad, 1992), and immunoelectron microscopic analyses of the sites of incorporation of biotinylated tubulin into MTs in axons also support this view (Okabe and Hirokawa, 1988).

A novel feature of composite MTs revealed by the present studies was that, in most cases, the proportion of tyr-tubulin within the tyr-tubulin-rich domains increased markedly from the transition towards the distal end (plus-end) of the MT in a complex and non-linear manner (see Figs 5, 7 and 9). This observation would not be expected if the rate of assembly of these domains was sufficiently rapid relative to the rate of detyrosination that essentially no detyrosination occurred during their growth, and if the tubulin carboxypeptidase had equal access to the MT all along its length. If both of these conditions applied, then we would expect to observe a constant proportion of tyr-tubulin throughout the tyr-tubulin-rich domain. Thus, our observation of a proximal-to-distal increase in tyr-tubulin content suggests that one or both of these conditions does not apply in these axons. For example, if detyrosination of the MT could occur during elongation, then the proximal region of these domains would contain fewer tyr-tubulin subunits that the distal region. If elongation occurred at a uniform rate and detyrosination occurred stochastically along the length of the growing polymer, then the amount of tyr-tubulin would be expected to increase exponentially from the minus-end to the plus-end of the tyr-tubulin-rich domain. Deviations from a simple exponential, which are indicated by the data (see Fig. 7 B, D), could reflect non-uniformities in the growth rate of the MTs. Implicit in this reasoning is the idea that the spatial variation in the tyr-tubulin content of the tyr-tubulin-rich domains reflects, in part, their previous growth behavior. If this is correct, then as more detailed information on the dynamics of MT assembly and detyrosination in living axons becomes available, it should be possible to interpret the spatial variation in tyr-

tubulin content along the length of individual MTs in terms of their life history.

We have used the frayed preparation to evaluate the tyr-tubulin content of MTs in the distal region of the axon and in growth cone. All of the MT profiles in the region of the growth cone stained strongly for tyr-tubulin. In many cases, we observed that these tyr-tubulin-rich MT profiles were in direct continuity with tyr-tubulin-poor profiles situated more proximally within the axon shaft, and the pseudocolor ratio images gave us the impression that this was so for all of the MT profiles in the region of the growth cone (see Fig. 5). Thus, all of the MT profiles in the region of the growth cone appear to represent the tyr-tubulin-rich domains of composite MTs that have their minus-ends situated more proximally, within the axon shaft. It is striking that tyr-tubulin-poor domains were observed only very infrequently in the region of the growth cone (see Figs 4 and 5). Furthermore, we did not observe any short MTs which could be traced from beginning to end within this region. While we cannot eliminate the possibility that such short MTs normally exist but were washed away during the extraction procedure, studies on MTs in living neurons have also suggested that MTs in the growth cone have their minus-ends situated more proximally (Sabry et al., 1991; Tanaka and Kirschner, 1991). The apparent absence of MTs that have their minus-ends located in the region of the growth cone suggests that little if any de novo formation of MTs occurs at this site. Nonetheless, this region represents one of the two principal regions within growing neurons where newly assembled polymer is concentrated (Brown et al., 1992; see below). These apparently conflicting results can be reconciled by proposing that the newly assembled polymer in the region of the growth cone forms by elongation of MTs situated more proximally, in the axon shaft (Baas and Black, 1990; Baas and Ahmad, 1992).

The data obtained with the frayed preparation also provide further insight into the regional differences in tyr-tubulin staining of MTs in axons. In a previous study, we showed that staining for tyr-tubulin in MT polymer is much greater in the proximal and distal regions of the growing axon than in the axon shaft (Brown et al., 1992). On the basis of the inverse relationship between the tyr-tubulin content of MTs and the age of these polymers (see above), we suggested that these regional differences in tyr-tubulin content reflected corresponding regional differences in the age of the MT polymer (Brown et al., 1992). Thus, we proposed that the youngest (most recently assembled) MT polymer in these growing axons is enriched in the proximal and distal regions compared to the axon shaft. The present studies confirm this basic staining pattern for tyr-tubulin in MTs. These observations, together with other studies from this laboratory using immunoelectron microscopy (Baas and Black, 1990; Baas et al. (1993), demonstrate that the regional differences in staining for tyr-tubulin are due, in part, to corresponding differences in the proportion of the total MT polymer that stains strongly for tyr-tubulin (see Figs 2 and 4). In addition, however, careful inspection of the images of frayed preparations revealed a subtlety to the tyr-tubulin staining patterns that was not apparent from our previous work. Specifically, we observed that the tyr-tubulin-rich polymer within the axon shaft generally stained less intensely than the tyr-tubulin-rich polymer present in the distal axon (see Fig. 2). A similar observation has been obtained independently by Ahmad et al. (1993) using immunoelectron microscopy. These observations raise the possibility that the tyr-tubulin-rich domains in the axon shaft have different assembly dynamics to those in the distal axon. Specifically, the tyr-tubulin-rich domains in the axon shaft may turn over more slowly, and therefore be older, than those in the region of the distal axon and growth cone. Similar regional differences in assembly dynamics were also proposed by Lim et al. (1989), based on studies that examined the time course of fluorescence recovery after photobleaching in different regions of the neurites of PC12 cells. Collectively, these observations indicate that mechanisms operate in neurons to regulate MT dynamics differentially as a function of location within the axon.

In conclusion, we have described a novel preparation that permits the visualization of individual axonal MTs of cultured neurons using conventional immunofluorescence procedures and epifluorescence microscopy. This preparation is uniquely suited for addressing questions that require the analysis of individual axonal MTs because relatively long lengths of individual MTs, together with their plus-ends, can be visualized readily. In the present studies, we have used this preparation to extend our understanding of the composite nature of axonal MTs. These studies have revealed an unexpected degree of complexity to the variation in tubulin composition along the length of individual MTs. We have suggested that the pattern of variation in the amount of tyr-tubulin and/or Ac-tubulin for any given MT represents a snapshot of its growth history. We are currently testing this possibility by microinjecting haptenized tubulin into neurons and then comparing the extent to which regions of individual MTs defined by differences in the amount of tyr-tubulin also differ in the extent to which they have incorporated the injected tubulin.

We thank Drs Chloe Bulinski and Giani Piperno for generously providing antibodies that were used in this study. This work was supported by a grant from the NIH to M.M.B.

REFERENCES

Ahmad, F.J., Pienkowski, T.P. and Baas, P.W. (1993). Regional differences in microtubule dynamics in the axon. *J. Neurosci.*, in press.

Baas, P.W. and Ahmad, F.J. (1992). The plus ends of stable microtubules are the exclusive nucleating structures for microtubules in the axon. *J. Cell Biol.* **116**, 1231-1241.

Baas, P.W. and Black, M.M. (1990). Individual microtubules in the axon consist of domains that differ in both composition and stability. *J. Cell Biol.* **111**, 495-509.

Baas, P.W., Slaughter, T., Brown, A. and Black, M.M. (1991). Microtubule dynamics in axons and dendrites. *J. Neurosci. Res.* **30**, 134-153.

Baas, P. W., Ahmad, F. J., Pienkowski, T. P., Brown, A. and Black, M. M. (1993). Sites of microtubule stabilization for the axon. *J. Neurosci.* in press.

Blose, S.H., Meltzer, D.I. and Feramisco, J.R. (1984). 10 nm filaments are induced to collapse in living cells microinjected with monoclonal and polyclonal antibodies against tubulin. *J. Cell Biol.* **98**, 847-858.

Bray, D. and Bunge, M.B. (1981). Serial analysis of microtubules of cultured rat sensory neurons. *J. Neurocytol.* **10**, 589-605.

Bré, M-H., Kreis, T. and Karsenti, E. (1987). Control of microtubule

nucleation and stability in Madin-Darby Canine Kidney Cells: the occurrence of non-centrosomal, stable detyrosinated microtubules. *J. Cell Biol.* **105**, 1283-1296.

Brown, A., Slaughter, T. and Black, M.M. (1992). Newly assembled microtubules are concentrated in the proximal and distal regions of growing axons. *J. Cell Biol.*, **119**, 867-882.

Cassimeris, L.U., Wadsworth, P. and Salmon, E.D. (1986). Dynamics of microtubule depolymerization in monocytes. *J. Cell Biol.* **102**, 2023-2032.

Gard, D.L. and Kirschner, M.W. (1987). Microtubule assembly in cytoplasmic extracts of *Xenopus* oocytes and eggs. *J. Cell Biol.* **105**, 2191-2201.

Gundersen, G.G., Khawaja, S. and Bulinski, J.C. (1987). Postpolymerization detyrosination of α-tubulin: A mechanism for subcellular differentiation of microtubules. *J. Cell Biol.* **105**, 251-264.

Higgins, D., Lein, P.J., Osterhout, D.J. and Johnson, M.I. (1991). Tissue culture of mammalian autonomic neurons. In *Culturing Nerve Cells* (ed. G. Banker and K. Goslin), pp. 177-205. MIT Press.

Kilmartin, J.V., Wright, B. and Milstein, C. (1982) . Rat monoclonal anti-tubulin antibodies derived by using a new non-secreting rat cell line. *J. Cell Biol.* **93**, 576-582.

Kreis, T. (1987). Microtubules containing detyrosinated tubulin are less dynamic. *EMBO J.* **6**, 2597-2606.

Kristoferson, D., Mitchison, T. and Kirschner, M. (1986). Direct observation of steady-state microtubule dynamics. *J. Cell Biol.* **102**, 1007-1019.

Lim, S-S., Sammak, P.J. and Borisy, G.G. (1989). Progressive and spatially differentiated stability of microtubules in developing neuronal cells. *J. Cell Biol.* **109**, 253-263.

Okabe, S. and Hirokawa, N. (1988). Microtubule dynamics in nerve cells: analysis using microinjection of biotinylated tubulin into PC12 cells. *J. Cell Biol.* **107**, 651-664.

Piperno, G. and Fuller, M.T. (1985). Monoclonal antibodies specific for an acetylated form of α-tubulin recognize antigens in cilia and flagella from a variety of organisms. *J. Cell Biol.* **101**, 2085-2094.

Sabry, J.H., O'Connor, T.P., Evans, L., Toroian-Raymond, A., Kirschner, M. and Bentley, D. (1991). Microtubule behavior during guidance of pioneer neuron growth cones *in situ*. *J. Cell Biol.* **115**, 381-395.

Schliwa, M. and van Blerkom, J. J. (1981). Structural interactions of cytoskeletal components. *J. Cell Biol.* **90**, 222-235.

Schulze, E., Asai, D. J., Bulinski, J.C. and Kirschner, M. (1987). Post-translational modification and microtubule stability. *J. Cell Biol.* **105**, 2167-2177.

Sherwin, T., Schneider, A., Sasse, R., Seebeck, T. and Gull, K. (1987). Distinct localization and cell cycle dependence of COOH-terminally tyrosinolated α-tubulin in microtubules of *Trypanosoma brucei*. *J. Cell Biol.* **104,** 439-446.

Sherwin, T. and Gull, K. (1989). Visualization of detyrosination along single microtubules reveals novel mechanisms of assembly during cytoskeletal duplication in trypanosomes. *Cell* **57**, 211-221.

Tanaka E. M. and Kirschner, M.W. (1991). Microtubule behavior in the growth cones of living neurons during axon elongation. *J. Cell Biol.* **115**, 345-363.

Wadsworth, P. and McGrail, M. (1990). Interphase microtubule dynamics are cell type-specific. *J. Cell Sci.* **95**, 23-32.

Walker, R.A., O'Brien, E. T., Pryer, N.K., Soboeiro, M.F., Voter, W.A., Erickson, H.P. and Salmon, E.D. (1988). Dynamic instability of individual microtubules analyzed by video light microscopy: rate constants and transition frequencies. *J. Cell Biol.* **107**, 1437-1448.

Webster, D.R., Gundersen, G.G., Bulinski, J.C. and Borisy, G.G. (1987). Differential turnover of tyrosinated and detyrosinated microtubules. *Proc. Nat. Acad. Sci.USA* **84**, 9040-9044.

Wehland, J., Willingham, M.C. and Sandoval, I.V. (1983). A rat monoclonal antibody reacting specifically with the tyrosylated form of -tubulin. I. Biochemical characterization, effects on microtubule polymerization *in vitro* and microtubule polymerization and organization *in vivo*. *J. Cell Biol.* **97**, 1476-1490.

Wehland, J. and Willingham, M.C. (1983). A rat monoclonal antibody reacting specifically with the tyrosylated form of α-tubulin. II. Effects on cell movement, organization of microtubules and intermediate filaments, and arrangement of Golgi elements. *J. Cell Biol.* **97**, 1476-1490.

Wehland, J. and Weber, K. (1987). Turnover of the carboxy-terminal tyrosine of α-tubulin and means of reaching elevated levels of detyrosination in living cells. *J. Cell Sci.* **88**, 185-203.

(Received 26 August 1992 - Accepted 28 October 1992)